UNCNET

Urban Europe and NSFC

Europe – China joint call on Sustainable Urbanisation in the Context of
Economic Transformation and Climate Change:
Sustainable and Liveable Cities and Urban Areas

Funded by
NCN (Poland), project UMO-2018/29 / Z / ST10 / 02986
NSFC (China), project 71961137011
FFG (Austria), project 870234

UNCNET

**Urban nitrogen cycles:
new economy thinking to master the challenges of climate change**

**D2/3: Using probability approaches to inform, revise and improve
contributions on the respective nitrogen flows**

Due date of deliverable: **30/11/2021**   Actual submission date: **18/2/2022**

Start Date of Project: **01/04/2019**   Duration: **35 months + 6 months**

Organisation name of co-chairs for this deliverable: **IIASA, CAS**

Authors: Samuel Guéret, Wilfried Winiwarter

Dissemination Level		
PU	Public	☒
PP	Restricted to other programme participants (including funding agencies)	☐
RE	Restricted to a group specified by the consortium (including funding agencies)	☐
CO	Confidential, only for members of the consortium (including funding agencies)	☐

1. Executive Summary

The current report aims to present a separate modeling framework using various probability approaches to inform, revise and improve the existing contributions on the Urban Nitrogen Budgets (UNBs) which are building on the final concept of the urban N flows exposed in the deliverable D2/2. Using Vienna Surrounding area as case study, the variability and uncertainty of the N flows have been assessed. On the one hand, a Linear Inverse Model has been implemented on the final UNB in STAN (WP 7). On the other hand, the Flux Variability Analysis approach has been combined with the use of Sampling Algorithms (SA) to derive comparable results with those produced by the STAN model.

2. Objectives:

The UNCNET project has been established to meet several challenges associated with urban nitrogen flows. Some of these challenges are explicit (linking different environmental spheres and problem areas via a common denominator, which in this case is reactive nitrogen; optimizing flowsvia circular economy approaches), others are more implicit (identifying appropriate system boundaries and comparable data sources; representing trade across such boundaries; developing strategies to represent changes that are more prevalent in dynamic urban situations than for a wholecountry). Building on the final version of the central model structure (D2/2) to be tested on such challenges, this report describes the Linear Inverse Model (LIM) framework of the final Urban Nitrogen Budget (UNB) using probability approaches to provide additional insight into the respective N flows in terms of variability and uncertainty and identify implementational opportunities. To that regard, both approaches of the Flux Variability Analysis (FVA) and of a Monte-Carlo Markov Chain (MCMC)-related Sampling Algorithm (SA) are respectively considered.

3. Activities:

Development of a LIM of the final UNB building on the STAN model structure

Use of probabilistic approaches to investigate variability and uncertainty of N flows

4. Results:

A linear inverse model of the final UNB has been established – see Annex

Probabilistic approaches have been utilized to provide insight on the N flows – see Annex

5. Milestones achieved:

---

6. Deviations and reasons:

Delay due to Corona crisis.

7. Publications:

---

8. Meetings:

---

9. List of Documents/Annexes:

Annex: A linear inverse model of the final urban nitrogen budget

The use of probabilistic approaches to provide insight on the N flows

10. Bibliography

ANNEX

A linear inverse model of the final urban nitrogen budget

Inverse methods have been widely used in the field of physical sciences for several decades (Parker 1977; Wunsch 1978; Wiggins 1972). These methods are introduced to process wide-ranging data from a given web structure and dynamics in order to estimate the range of specific unknown flows. Here model parameters are inferred from the data, hence the method is referred to as "inverse" model. While, in common experiments, a model is generally used to derive the evolution of state variables from initial conditions and other known parameter values; the reverse happens when using inverse methods as parameters are this time estimated from the result, the state variables. Linear Inverse Models (LIMs) are particular subsets of inverse methods. Flow estimates in LIMs are derived within time and space domains over which the set of constraints used are limited to linear combinations (Vézina and Piatt 1988). In the present case of interest, the web structure, dynamics and unknowns are the N topology matrix, the model input data and the N flows carried between the different pools, respectively (van Oevelen et al. 2010).

The estimation of network flows through LIMs is particularly effective in the case of underdetermined networks which are defined by a number of unknown flows higher than the available linear equality constraints (mass balances and empirical data from measurements) relating them.

LIMs only require the knowledge of the network topology - that is, how the flows and pools are interconnected - for the input data to be implemented. The current state of the network topology of Vienna surrounding area's UNB for the base year 2015 is shown as a compact table matrix in the following Figure 1. The abbreviations of the various pools defined in the Figure's caption shall be used throughout the deliverable.

Being especially useful for underdetermined networks, the LIM implementation of UNBs is foreseen to potentially provide valuable results when deriving historical data-related UNBs for which more unknown N flows than for the 2015 base year are to be expected. Building on the results of WP7, the Vienna surrounding area's UNB for the year 2015 for which much input data is already known is therefore used as a case-study throughout the present report.

to

	AIR	WW	WAT	WAS	HH	AGL	HOR	URG	LIV	PET	IND	COM	IMX	OUT
AIR	0	0	0	0	0	F1	F2	F3	0	0	0	0	F4	0
WW	F5	0	F6	F7	0	F8	0	0	0	0	0	0	0	0
WAT	0	0	0	0	0	F9	F10	F11	0	0	0	0	F12	0
WAS	F13	0	0	0	0	F14	0	F15	0	0	F16	F17	F18	0
HH	0	F19	0	F20	0	0	0	F21	0	0	0	F22	0	0
AGL	F23	0	F24	F25	F26	0	0	0	F27	0	F28	F29	F30	0
HOR	F31	0	F32	F33	F34	0	0	F35	0	0	0	0	F36	0
URG	F37	0	F38	F39	0	0	0	0	0	0	0	0	0	0
LIV	F40	F41	0	F42	F43	F44	0	0	0	0	F45	0	F46	0
PET	F47	0	0	F48	0	0	0	F49	0	0	0	0	F50	0
IND	0	F51	0	F52	F53	F54	F55	F56	F57	F58	0	F59	F60	0
COM	F61	0	0	0	0	0	0	0	0	0	0	0	0	0
IMX	F62	F63	0	0	0	0	F64	0	F65	F66	F67	0	0	F68
OUT	0	0	0	0	0	0	0	0	0	0	0	0	F69	0

from

Figure 1 - UNB Topology matrix of the Vienna surrounding area for the base year 2015 indicating the flows (flow numbers refer to detailed explanation given in Appendix A). Rows represent the originating pools and columns the recipient ones. AIR = Air; WW = Wastewater; WAT = Water; WAS = Waste; HH = Households; AGL = Agricultural land; HOR = Horticulture; URG = Urban green; LIV = Livestock; PET = Pets; IND = Industry; COM = Combustion; IMX = Import/Export; OUT = Outside boundaries

Inverse problems are generally modelled through difference equations that are specific functions of the state variables and the unknown parameters (Vézina and Piatt 1988).

When data available on the network dynamics are insufficient, a steady-state regime assumption reflecting a null net change of matter is usually taken in each pool over the considered time period. Under such assumption, the linear inverse problem of the Viennese UNB can mathematically be described under the form of the following compact matrix equation and inequations:

$$A \cdot r = b = 0$$

(1)

$$G \cdot r \leq h$$

(2)

$$r \geq 0$$

(3)

Where – for m, n and p representing the number of mass-balance equations, unknown N flows and inequality constraints –

- **A** is the (m x n) state matrix characterizing the average network state;
- **r** is the (n x 1) vector of the unknowns which therefore gathers the 69 unknown N flows of the UNB (see Appendix A);

- The (m x 1) **b** vector, whose i[th] element is representative of the temporal change of mass of a given pool i, is here equivalent to the null vector **0** given the steady-state assumption stated above;
- **G** is a (p x n) matrix of coefficients linking together the different unknown N flows gathered in the **r** vector;
- **h** is the (p x 1) vector of the inequality conditions which gathers the 99 inequality constraints of the UNB (see Appendix B).

While Equ. (1) portrays an equality matrix equation gathering the system of the 13 mass-balance equations representative of the 13 pools of the budget (excluding the OUT pool), softer constraints are incorporated in the Equ. (2) via inequalities for which linear combinations of the N flows are constrained by a specific lower or upper bound. This allows the incorporation of lower quality data (e.g. from the literature or poorer measurements) into the budget model and thus more comprehensive and realistic flow estimates (Kones et al. 2006).

In the case of the Viennese UNB, the implementation of the 99 inequality constraints builds on the results of the final UNB from WP 7 implemented in STAN. The lower and upper bounds of such constraints are directly derived from the available input data for STAN and equal the input flow value $\pm$ two times its standard deviation. Some additional inequality constraints consisting of more complex linear combinations of the flows are further detailed in Table 2 of the report (see later in this report, in the section dedicated to the sensitivity analysis of the compost case study).

Finally, the Equ. (3) refers to a default set of inequations ensuring that flow directions are consistent with the network topology (see Figure 1).

The use of probabilistic approaches to provide insight on the N flows

Starting from the LIM implemented on the UNB of Vienna, several methods exist that provide further insight onto the N flows and address potential issues of underdetermined parameters. In the present deliverable we consider FVA and SA, still using the 2015 UNB of the Vienna surrounding area as a case study.

The FVA approach refers to the use of linear programs to provide the lower and upper bounds of each of the network flows and is carried out first. Subsequently, SAs are discussed, which allow, among other things, the derivation of statistically representative solutions (e.g. mean flows solution) and marginal distributions of each of these flows upon the sampling of the admissible solution space.

Flux Variability Analysis

The Flux Variability Analysis refers to the use of Linear Programs (LPs) to provide the lower and upper bounds of each of the network flows, hence directly characterizing the solution space (Gudmundsson and Thiele 2010; Mahadevan and Schilling 2003). The idea behind it is to sequentially minimize and maximize each of the flows of the network subject to the set of constraints characterizing the LIM (cf. Eqs. (1)-(3)) through linear programming techniques. This is mathematically summarized as follows:

$$
\begin{matrix} \min r_i \\ \max r_i \end{matrix} \quad \forall i \in [1, \dots, 69] \quad s.t. \quad \begin{cases} \boldsymbol{A}.\boldsymbol{r} = \boldsymbol{0} \\ \boldsymbol{G}.\boldsymbol{r} \leq \boldsymbol{h} \\ \boldsymbol{r} \geq \boldsymbol{0} \end{cases}
$$

$$(4)$$

Where $\min r_i$ and $\max r_i$ respectively refer to the minimization and maximization of the ith element of the (69 x 1) vector r, that is, of the ith unknown N flow r_i (i =1,...,69). For the considered LIM of the Viennese UNB, the linprog solver using a dual-simplex algorithm from Matlab was used to successively solve the 2 * 69 LPs.

The following Figure 1 displays the overall magnitude distribution of the minimum and maximum admissible values of the UNB's 69 N flows upon solving the above set of LPs. A zoom is provided for the flows F31 to F38 where values are too small to be detected using the overall Figure's scale.
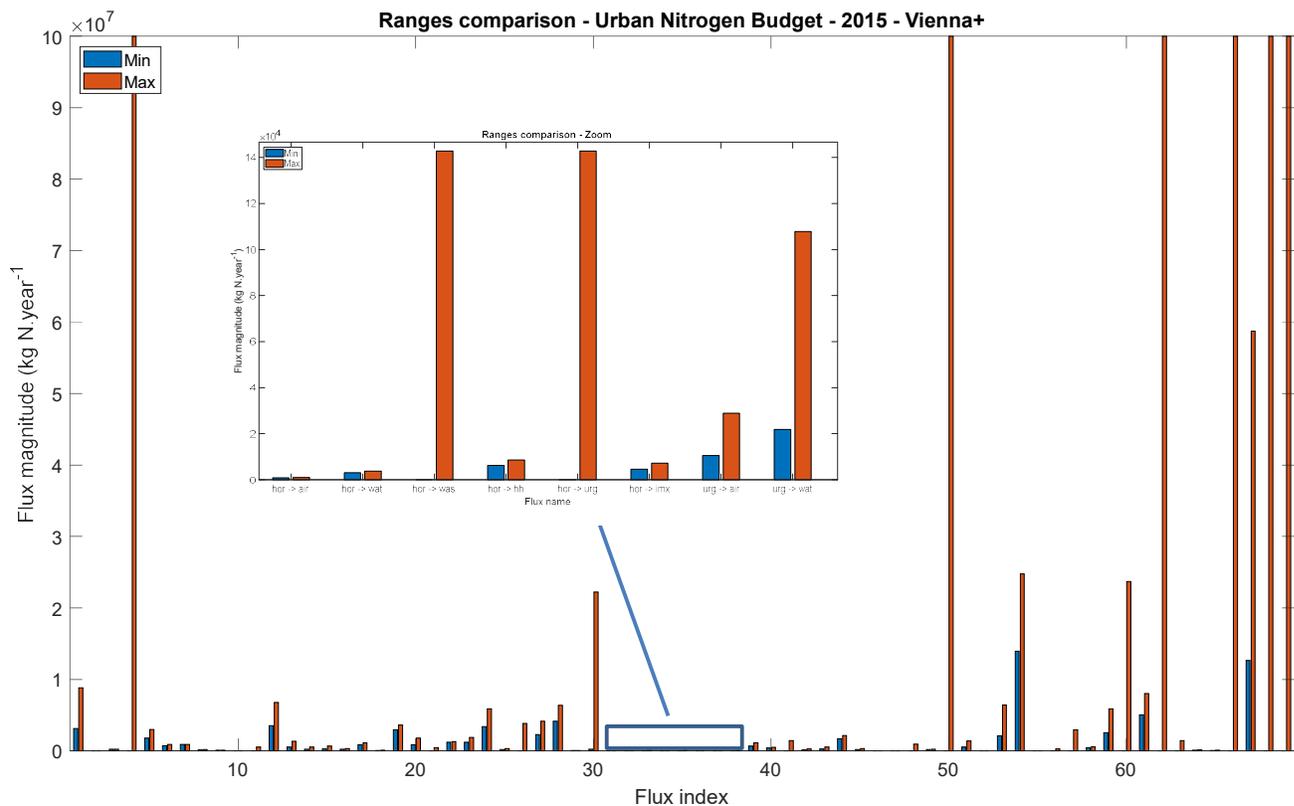
Figure 2 – Minimum and maximum admissible values for the 69 N flows of the Viennese UNB for the base year 2015. Blue bars refer to the minimum admissible value; Red bars refer to the maximum admissible value.

We can first discuss the variability of the respective flows in the UNB. First of all, unconstrained flows range from the absolute minimum value of 0 to the set maximum of 1E+08 kg N.year^{-1}. But also constraints themselves may have large ranges. Upper constraints (see red bars in Figure 2) span more than 3 orders of magnitude, ranging from 1.0 E+04 kg N.year^{-1} (F31 HOR → AIR) to 5.9 E+07 kg N.year-1 (F67 IMX → IND). Lower constraints (see blue bars in Figure 2) differ even more, with extreme values (excluding null-flow values) ranging from 8.3 E+02 kg N.year^{-1} (F10 WAT → HOR) to 1.4 E+07 kg N.year^{-1} (F54 IND → AGL).

Not only the minimum and maximum values in the magnitude profiles vary widely, but also the flow ranges themselves differ. Indeed, the admissible flow ranges extend from 1.7 E+02 kg N.year^{-1} (narrowest range – F31 HOR → AIR) to 4.6 E+07 kg N.year^{-1} (widest range – F67 IMX → IND), spanning across more than 5 orders of magnitude.

As already noted, a few flows – all of which being related to the "Import/Export" pool -remain completely unconstrained despite the constraints implemented. They span the entire arbitrary space of flow threshold values (0 to 1 E+08 kg N.year^{-1}). These correspond to the red bars reaching the top of the frame in the above Figure 2. Such flows, arising by insufficient system constraints, should therefore be considered irrelevant in their present state.

Despite the fact most of the inequality constraints are directly derived from STAN input data, a number of flow ranges differ between the FVA and STAN outputs, as seen in the following Table 1:

Table 1 – Flow range differences between the Flux Variability Analysis and STAN outputs

Flow name	STAN (kg N.year^{-1})	FVA (kg N.year^{-1})
F5 WW → AIR	[1.77 E+06; 2.88 E+06]	[1.81 E+06; 2.97 E+06]
F11 WAT → URG	[0;0]	[0; 5.29 E+05]
F12 WAT → IMX	[4.68 E+06; 7.68 E+06]	[3.54 E+06; 6.79 E+06]
F20 HH →WAS	[8.79 E+05; 1.91 E+06]	[8.79 E+05; 1.81 E+06]
F21 HH → URG	[0; 1.38 E+06]	[0; 4.50 E+05]
F23 AGL → AIR	[1.25 E+06; 1.66 E+06]	[1.20 E+06; 1.88 E+06]
F24 AGL → WAT	[3.78 E+06; 6.76 E+06]	[1.20 E+06; 1.88 E+06]
F27 AGL → LIV	[2.56 E+06; 3.87 E+06]	[2.29 E+06; 4.15 E+06]
F33 HOR → WAS	[0; 0]	[0; 1.43 E+05]
F35 HOR → URG	[0; 0]	[0; 1.43 E+05]
F37 URG → AIR	[3.30 E+05; 1.03 E+06]	[1.05 E+04; 2.89 E+04]
F38 URG → WAT	[1.02 E+05; 3.30 E+05]	[2.18 E+04; 1.08 E+05]
F48 PET → WAS	[0; 0]	[0; 9.30 E+05]
F53 IND →HH	[2.10 E+06; 6.52 E+06]	[2.10 E+06; 6.42 E+06]
F57 IND → LIV	[0; 0]	[0; 2.94 E+06]
F63 IMX → WW	[0; 0]	[0; 1.45 E+06]
F67 IMX → IND	[4.55 E+07; 6.10 E+07]	[1.26 E+07; 5.88 E+07]

As a first remark, it can be mentioned that a few flows for which null ranges are generated by STAN due to lack of data are actually given a non-null range through the FVA approach.

Among the flow ranges in Table 1 above, it is noteworthy to outline that some of them, (e.g. related to F20 or F53), differ only slightly (about 100 ton N of difference for the sole upper bound), while other ones (e.g. related to F37 or F67) deviate more strongly. Some discrepancies associated to volatilization and leaching from AGL (F23-24) and URG (F37-38) pools can be explained through the introduction of the related supplementary inequality constraints in the UNB's LIM. This is shown in more detail in

Table 2 (next section, sensitivity analysis of the compost case study). Most of the other discrepancies (excluding those pertaining to null-flow values from STAN) seem justified by the post-computational adjustment of the flow uncertainties in STAN following the error propagation approach.

Despite such discrepancies, the FVA remains a useful tool to characterize the boundaries of the solution space and to derive flow ranges which cannot be produced through the STAN model. In particular, the latter feature is foreseen to work best in underdetermined conditions. Further research is needed to supply the model with additional multi-flow-linking constraints.

Sampling Algorithms

In the field of probabilistic inference, Sampling Algorithms (SA) have long proved to be particularly relevant tools to probe and induce features of underdetermined networks. As examples, a few of the numerous works in the metabolic networks- and food web-related literature can be referred to (Almaas et al. 2004; Gomes de Oliveira Dal'Molin et al. 2015; Price, Schellenberger, and Palsson 2004; Bordel, Agren, and Nielsen 2010; Pacella et al. 2013; Subbey, Benjamin, and Lindstrøm 2016).
In addition to the FVA approach characterizing the solution space, various other aspects of underdetermined networks can be investigated using SAs. In the present case of interest, they notably permit the uniform random sampling of the solution space and the generation of the Marginal Distributions (MDs) of each of the UNB's flows. Also, particular solutions (e.g., the average solution) can be extracted out of the finite randomly generated solutions and compared to those produced by the STAN model.

Regarding the approach itself, a first linear transformation step allowing the elimination of the LIM equality constraints is in practice often performed. The solution space to be sampled is consequently characterized by a convex polytope delineated by the intersections of hyperplanes representative of the inequality constraints of the LIM.

The R-package "LIM", specifically designed for reading and solving LIMs in the context of flow and reaction networks, was used to sample the LIM implementation of Vienna surrounding area's UNB for the base year 2015 subject to the set of Eqs. (1-(3). That package includes the xsample() function using a MCMC-related SA termed as the "Mirror Algorithm" (MA) to build the MDs of each of the N flows (Soetaert, Van den Meersche, and Oevelen 2009). For that purpose, the various sampling-related results discussed below are all produced using a Markov chain constituted by a total of 1500 sample points.

Eventually, we note that numerous other SAs of varying ease of implementation and/or computational efficiency exist in the literature (Rubinstein 1982; Smith 1984; Haraldsdóttir et al. 2017; Bogaerts and Rooman 2021). The analysis of their advantages and drawbacks with respect to the MA, however, exceeds the scope of the present deliverable and therefore is not addressed.

Marginal Distributions and Pairwise Scatter Plots

As additional valuable feature to MDs, Pairwise Scatter Plots (PSPs) can be generated. They are linking together the MDs of two given N flows to assess their relative degree of correlation. In practice, the MDs of a given pair of flows are thus obtained projecting the corresponding PSP onto these flows' axes.

For example, the following
Figure 3 displays on the diagonal line the MDs of the N flows associated with WAT and HOR pools along with the corresponding PSPs underneath it. The respective correlation coefficients, quantitatively characterizing the relative degree of correlation conveyed by each PSP, are also shown. These are displayed symmetrically to the corresponding PSP with respect to the diagonal line.
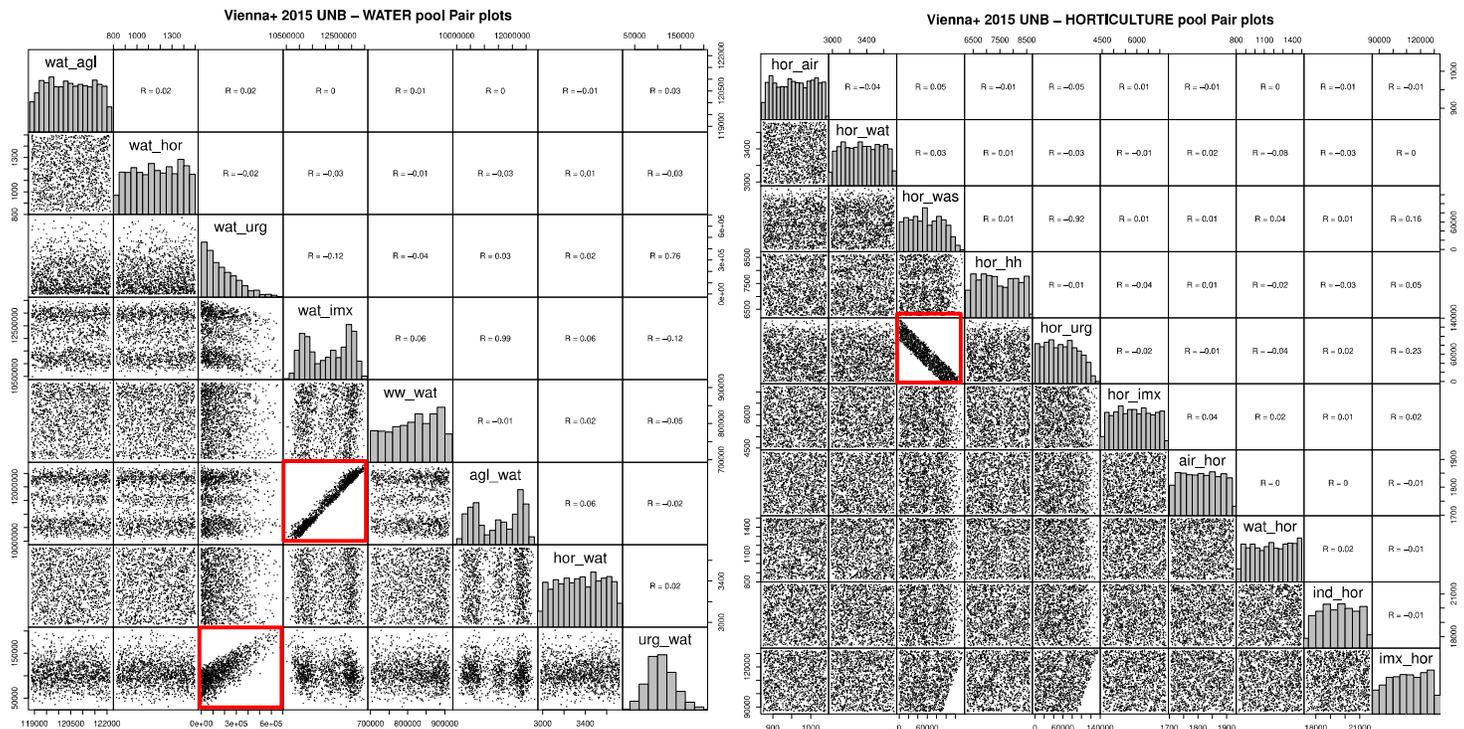

Figure 3 – Marginal distributions and Pairwise scatter plots of the N flows in kg N.year^{-1} associated with the Water and Horticulture pools along with the corresponding correlation coefficients. Red rectangles indicate significant correlations for which $|R| \geq 0.75$.

As seen in the above
Figure 3, MDs of the individual flows of WAT and HOR pools exhibit widely variable patterns. No particular distribution patterns was therein recognized that could be associated with a given pool, type of flow (i.e. in/outflow), or specific inherent physical process. Similar conclusions are drawn when carrying out the simulation analysis for the rest of the pools of the UNB.

The investigation of the PSPs additionally leads to the findings of several outstanding correlations between given pairs of N flows, such as those enclosed by red rectangles in the above
Figure 3. We have observed two main types of outcomes when looking for physical and/or (eco-)physiological interpretations of such strongly correlated flows: either (a) the correlation is strong to very strong ($0.75 \leq |R| < 1$) and related to flows constrained by at least one constraint from the set of inequality constraints from Equ. (2, or (b) the correlation is very strong to perfect ($0.9 \leq |R| \leq 1$) and none of the related flows is constrained by an inequality constraint. Such outcomes are specifically exemplified in the following Figure 4 looking into more detail to some of the enclosed correlations of the above
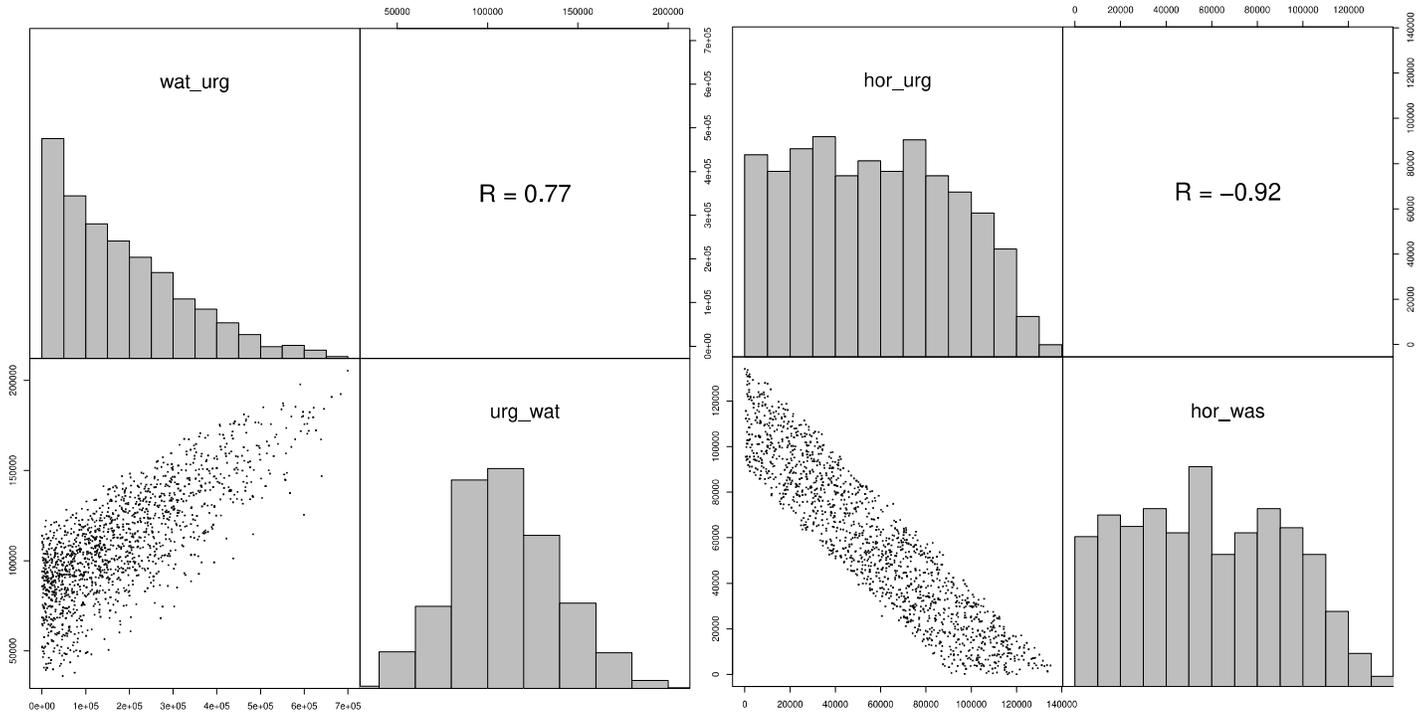Figure 3.

Figure 4 - Marginal distributions (top left and bottom right) and Pairwise scatter plots (bottom left) of the N flow pairs WAT → URG / URG → WAT (left) and HOR → URG / HOR → WAS (right) in kg N.year⁻¹ along with the corresponding correlation coefficients (top right)

The above Figure 4 displays the MDs of the two N flow pairs F11 WAT → URG / F38 URG → WAT and F33 HOR → WAS / F35 HOR → URG along with the two correlations characterized by their respective PSPs. We can first note that the flow F38 URG → WAT on the left panel is constrained by an additional leaching equality constraint, as shown in more detail in

Table 2 (next section, sensitivity analysis of the compost case study). The corresponding positive correlation (R=0.77) further suggests a plausible increase of N leaching with the increase of irrigation to the urban green pool.

The two flows on the right panel suggest an increase of horticultural products in urban green areas with the reduced waste of horticultural products. Upon closer scrutiny of the HOR pool, it appears that these two flows are the only ones of the pool that are only constrained through the mass-balance equations (cf. Equ. 1) and that are given identical admissible ranges by the solver. In that case, the strong correlation (R=-0.92) suggests that N is either flowing to the HOR or the URG pool. Yet, we note that the consistency of the correlation in that tier is not always guaranteed.

Out of the two outcomes discussed above, a higher number of them belong to tier (b) than to tier (a). Therefore, we foresee that the generation of multi-flow linking constraints increasing the overall degree of constraint of the budget would help provide even more exploitable results from the simulations.

Particular solutions: Comparison with STAN output

In the case of underdetermined networks, SAs may also be used to derive particular solutions out of the finite randomly generated solutions following the sampling of the solution space. Here, mean MCMC solutions were computed using the respective ldei() and xsample() functions of the LIM package in R (Soetaert, Van den Meersche, and Oevelen 2009). Specifically, the ith N flow value (i=1,...,69) was determined by computing the arithmetic mean of the 1500 sample points forming the ith column of the (1500 x 69) solution matrix produced by xsample().
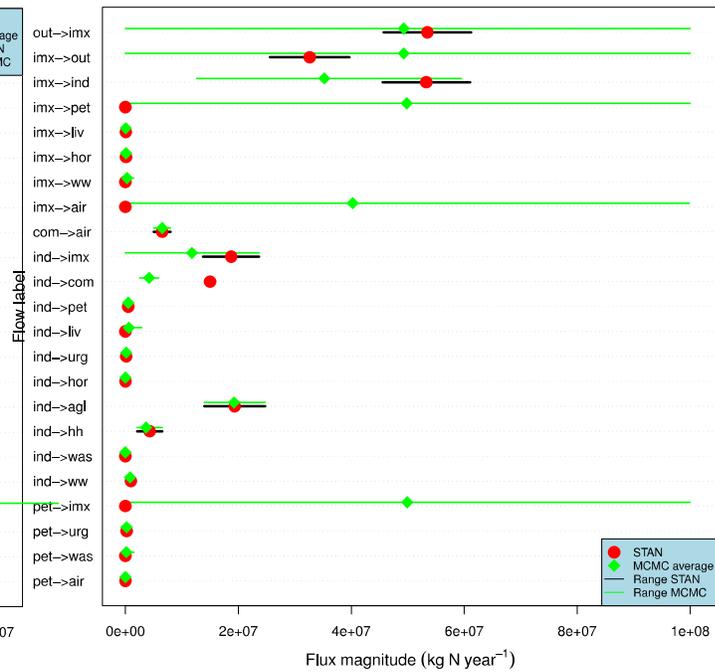
The following Figure 5 (a)-(c) display dot charts of both the STAN and mean MCMC particular solutions of the Vienna surrounding area's UNB for the base year 2015. The corresponding computed admissible ranges are shown along in both cases.
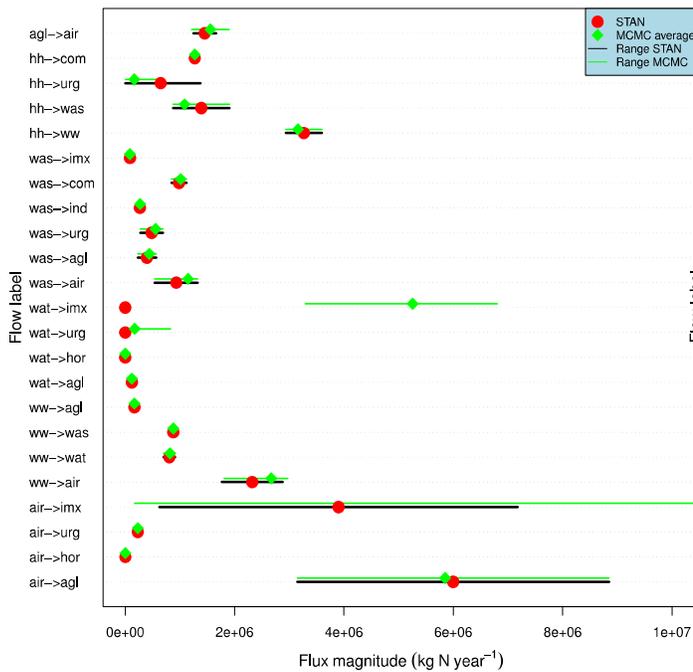
(a) N flows F1 to F23

(b) N flows F24 to F46
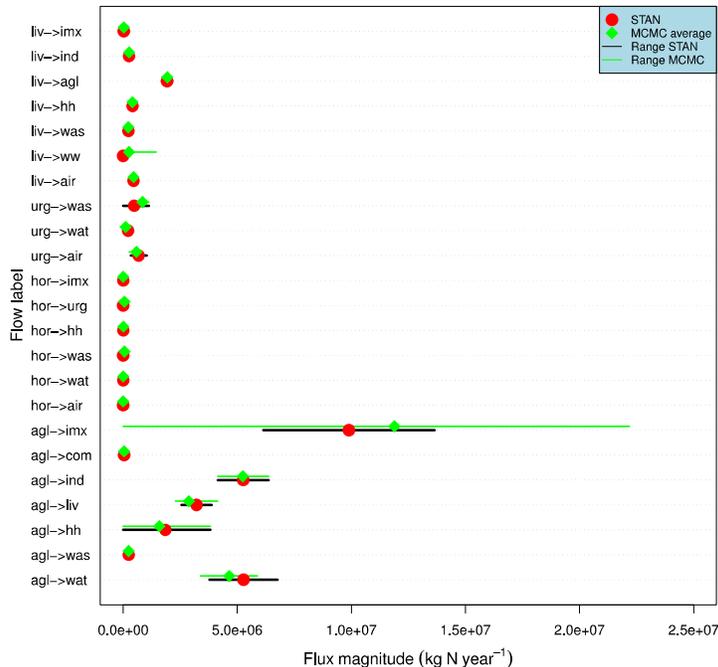
(c) N flows F47 to F69

Figure 5 – Dot charts of the STAN and average MCMC solutions in kg N.year⁻¹ of Vienna surrounding area's UNB for the base year 2015. The black and green lines respectively indicate the admissible range of each corresponding N flow. Red circles and green diamonds respectively refer to the STAN and average MCMC computed flow values.

In the above Figure 5, we first note that both approaches, STAN and the MCMC-related SA, globally yield comparable results. When the respective particular N solutions are not strictly superimposing, the discrepancies can be explained in three major ways:

1. The flow is unconstrained for at least one of the two approaches (e.g. F4 AIR → IMX);
2. The flows have very similar to identical ranges in both cases but different solutions due to the non-centered distribution of the MCMC-related approach (e.g. F20 HH → WAS);
3. The flow is set to zero in STAN due to lack of data (see Table 1) but is given a particular solution and is constrained in the MCMC-related approach (e.g. F11 WAT → URG)

Case (1.) highlights the need of refining the equation/inequation matrix system (see Eqs. (1)-(3)) to reduce the number of unconstrained flows; cases (2.) and (3.) demonstrate the potential benefits from using the SA approach. While case (2.) challenges the precision of the solution generated in STAN; case (3.) might prove valuable for stronger underdetermined UNB for which more N flows are expected to be unknown.

Sensitivity Analysis: Compost case study

For improved interpretation of SA results, we performed a sensitivity analysis by varying input parameters. Specifically, we select a case study aiming to assess potential adverse or beneficial environmental effects upon varying the N input of compost in the AGL pool (i.e. F14 WAS → AGL). This parameter is expected to be relevant for volatilization, leaching, and for fertilizer inputs.

We proceeded as follows: two extreme cases are implemented, for which 5% or 95%, respectively, of the total available compost are sent to the AGL pool, and results are compared to the baseline. In each scenario, the remaining available compost is allocated to the URG pool.

This required to remove the inequality constraints of both flows F14 (WAS → AGL) and F15 (WAS → URG) from the inequation matrix (cf. Equ. (2)) to allow the new compost inputs exceed their previously admissible ranges. That required to introduce new constraints, relative to the total available compost (sum of F14 and F15, cf. Table 2 below), so that results remained in reasonable bounds: the bounds of these new constraints were taken from the sum of the respective bounds of the initial flows. Likewise, the inequality constraints of volatilization and leaching N flows from the pools AGL (F23 and F24, respectively) and URG (F37 and F38, respectively) - which depend on the compost inputs - were replaced by equality constraints spotlighting such dependencies. Parameters in these equations reflect the underlying allocation of flows. Eventually, the former inequality constraints of the fertilizer input to the AGL pool (F54 ind → agl) were also removed to allow the new results to potentially exceed the previously admissible ranges.

These changes are summarized in the following Table 2, where:

- the [lower bound, upper bound] terms refer to the respective lower and upper bounds assigned as inequality constraints to the (group of) flows considered);
- The " – " signs refer to unconstrained (group of) flows;
- The other terms assign flows as equality constraints.

Table 2 – Summary of the equation/inequation matrix changes pertaining to the compost sensitivity analysis.

(Group of) flow(s)	Baseline	5% Compost input	95% Compost input
F14 WAS → AGL	[227680, 565612]	0.05 * 881436	0.95 * 881436
F15 WAS → URG	[278276, 691303]	–	–
F14 WAS → AGL + F15 WAS → URG	–	[505956, 1256914]	
F23 AGL → AIR	[1246874, 1661125]	0.06*F8+ 0.03*F14 + 0.295*F44 + 0.05*F54	
F24 AGL → WAT	[3783143, 6763707]	0.227*(F8+F14) + 0.159*F44 + 0.217*F54	
F37 URG → AIR	[329504, 1028161]	0.033 * F15 + 0.027 * F56	
F38 URG → WAT	[102246, 330480]	-0.097*F3 + 0.15*F11 + 0.15*F15 + 0.15*F56	
F54 IND → AGL	[13955244, 24749492]	–	

We can now focus on the environmental effects generated in either case. The results of this sensitivity analysis for the AGL pool are presented in the following Figure 6, separately displaying for each of the three cases the MDs and PSPs of the flows related to volatilization, leaching, and fertilizer inputs:

Figure 6 – MDs and PSPs of the volatilization- (AGL → AIR), leaching- (AGL → WAT), and fertilizer input- (IND → AGL) related flows of the AGL pool for the baseline (top) and the cases of 5% (top right) and 95% (right) of the total available compost used as input in the AGL pool(WAS → AGL).

As shown in the above Figure 6, the increase (resp. decrease) with respect to the baseline of compost input to the AGL pool to 95% (resp. 5%) of the total available compost decreases (resp. increases) the average flow values relative to the volatilization, leaching and fertilizer inputs. The resulting values average flow are quantitatively summarized in the Table 3 below.

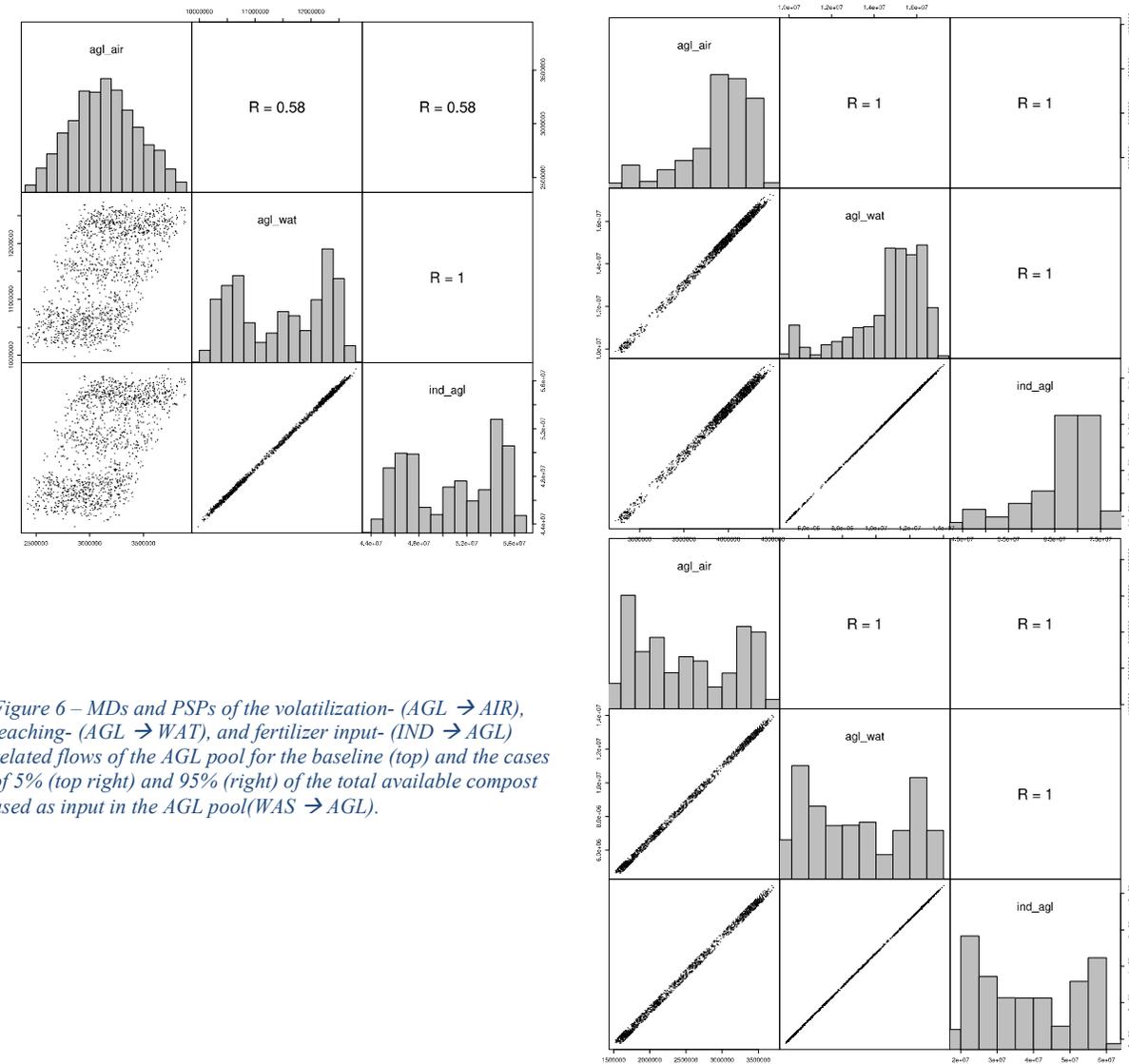*Table 3 – Average flow values in kg N.year^{-1} for the baseline and compost input variation cases of the volatilization- (agl → air), leaching- (agl → wat) and fertilizer input- (ind → agl) related flows for the AGL pool.*

Flow	Average flow value		
	Baseline	5% compost input	95% compost input
AGL → AIR	3.14 E+06	3.89 E+06	2.51 E+06
AGL → WAT	1.15 E+07	1.47 E+07	8.81 E+06
IND → AGL	5.08 E+07	6.62 E+07	3.81 E+07

These findings support the claim of reduced environmental effects when the share of compost increases in the AGL pool.

The use of sensitivity analyses with respect to various input parameters can provide valuable assessments of the uncertainties on the predicted model output. Hence, they do appear promising to explore the characteristics of the other research areas' UNBs in not fully determined conditions. Yet, as seen with the FVA approach and previous applications of the SAs to the UNB's LIM, additional efforts need to be carried out to provide more realistic and exploitable results. Specifically, further research is suggested towards deriving new multi-flow-linking constraints. These constraints might originate from the literature or from reasonable eco-physiological assumptions.

Bibliography

Almaas, E., B. Kovács, T. Vicsek, Z. N. Oltvai, and A.-L. Barabási. 2004. "Global Organization of Metabolic Fluxes in the Bacterium Escherichia Coli." *Nature* 427 (6977): 839–43. https://doi.org/10.1038/nature02289.

Bogaerts, Philippe, and Marianne Rooman. 2021. "DISCOPOLIS 2.0: A New Recursive Version of the Algorithm for Uniform Sampling of Metabolic Flux Distributions with Linear Programming." *IFAC-PapersOnLine*, 16th IFAC Symposium on Advanced Control of Chemical Processes ADCHEM 2021, 54 (3): 300–305. https://doi.org/10.1016/j.ifacol.2021.08.258.

Bordel, Sergio, Rasmus Agren, and Jens Nielsen. 2010. "Sampling the Solution Space in Genome-Scale Metabolic Networks Reveals Transcriptional Regulation in Key Enzymes." *PLOS Computational Biology* 6 (7): e1000859. https://doi.org/10.1371/journal.pcbi.1000859.

Gomes de Oliveira Dal'Molin, Cristiana, Lake-Ee Quek, Pedro A. Saa, and Lars K. Nielsen. 2015. "A Multi-Tissue Genome-Scale Metabolic Modeling Framework for the Analysis of Whole Plant Systems." *Frontiers in Plant Science* 6: 4. https://doi.org/10.3389/fpls.2015.00004.

Gudmundsson, Steinn, and Ines Thiele. 2010. "Computationally Efficient Flux Variability Analysis." *BMC Bioinformatics* 11 (September): 489. https://doi.org/10.1186/1471-2105-11-489.

Haraldsdóttir, H., Benjamin R. Cousins, I. Thiele, R. Fleming, and S. Vempala. 2017. "CHRR: Coordinate Hit-and-Run with Rounding for Uniform Sampling of Constraint-Based Models." *Bioinform.* https://doi.org/10.1093/bioinformatics/btx052.

Kones, Julius K., Karline Soetaert, Dick van Oevelen, John O. Owino, and Kenneth Mavuti. 2006. "Gaining Insight into Food Webs Reconstructed by the Inverse Method." *Journal of Marine Systems* 60 (1–2): 153–66. https://doi.org/10.1016/j.jmarsys.2005.12.002.

Mahadevan, R., and C. H. Schilling. 2003. "The Effects of Alternate Optimal Solutions in Constraint-Based Genome-Scale Metabolic Models." *Metabolic Engineering* 5 (4): 264–76. https://doi.org/10.1016/j.ymben.2003.09.002.

Oevelen, Dick van, Karel Van den Meersche, Filip J. R. Meysman, Karline Soetaert, Jack J. Middelburg, and Alain F. Vézina. 2010. "Quantifying Food Web Flows Using Linear Inverse Models." *Ecosystems* 13 (1): 32–45. https://doi.org/10.1007/s10021-009-9297-6.

Pacella, Stephen R., Benoit Lebreton, Pierre Richard, Donald Phillips, Theodore H. DeWitt, and Nathalie Niquil. 2013. "Incorporation of Diet Information Derived from Bayesian Stable Isotope Mixing Models into Mass-Balanced Marine Ecosystem Models: A Case Study from the Marennes-Oléron Estuary, France." *Ecological Modelling* 267 (October): 127–37. https://doi.org/10.1016/j.ecolmodel.2013.07.018.

Parker, R L. 1977. "Understanding Inverse Theory." *Annual Review of Earth and Planetary Sciences* 5 (1): 35–64. https://doi.org/10.1146/annurev.ea.05.050177.000343.

Price, Nathan D., Jan Schellenberger, and Bernhard O. Palsson. 2004. "Uniform Sampling of Steady-State Flux Spaces: Means to Design Experiments and to Interpret Enzymopathies." *Biophysical Journal* 87 (4): 2172–86. https://doi.org/10.1529/biophysj.104.043000.

Rubinstein, R. Y. 1982. "Generating Random Vectors Uniformly Distributed inside and on the Surface of Different Regions." *European Journal of Operational Research* 10 (2): 205–9. https://doi.org/10.1016/0377-2217(82)90161-8.

Smith, Robert L. 1984. "Efficient Monte Carlo Procedures for Generating Points Uniformly Distributed Over Bounded Regions." *Operations Research* 32 (6): 1296–1308.

Soetaert, K., Karel Van den Meersche, and D. Oevelen. 2009. "Package LimSolve , Solving Linear Inverse Models in R," January.

Subbey, Sam, Planque Benjamin, and Ulf Lindstrøm. 2016. "Exploring Stochasticity and Imprecise Knowledge Based on Linear Inequality Constraints." *Journal of Mathematical Biology* 73 (September). https://doi.org/10.1007/s00285-015-0959-z.

Vézina, Af, and T Piatt. 1988. "Food Web Dynamics in the Ocean. I. Best-Estimates of Flow Networks Using Inverse Methods." *Marine Ecology Progress Series* 42: 269–87. https://doi.org/10.3354/meps042269.

Wiggins, Ralph A. 1972. "The General Linear Inverse Problem: Implication of Surface Waves and Free Oscillations for Earth Structure." *Reviews of Geophysics* 10 (1): 251–85.

https://doi.org/10.1029/RG010i001p00251.

Wunsch, C. 1978. "The North Atlantic General Circulation West of 50/Sup 0/W Determined by Inverse Methods." *Rev. Geophys. Space Phys.; (United States)* 16:4 (November). https://doi.org/10.1029/RG016i004p00583.

Appendix A – Flow numbers used in the UNB Topology Matrix (see Figure 1) along with their detailed explanation.

Flow number	Flow name
F1	Air to Agricultural land
F2	Air to Horticulture
F3	Air to Urban green
F4	Air to Import/Export
F5	Wastewater to Air
F6	Wastewater to Water
F7	Wastewater to Waste
F8	Wastewater to Agricultural land
F9	Water to Agricultural land
F10	Water to Horticulture
F11	Water to Urban green
F12	Water to Import/Export
F13	Waste to Air
F14	Waste to Agricultural land
F15	Waste to Urban green
F16	Waste to Industry
F17	Waste to Combustion
F18	Waste to Import/Export
F19	Households to Wastewater
F20	Households to Waste
F21	Households to Urban green
F22	Households to Combustion
F23	Agricultural land to Air
F24	Agricultural land to Water
F25	Agricultural land to Waste
F26	Agricultural land to Households
F27	Agricultural land to Livestock
F28	Agricultural land to Industry
F29	Agricultural land to Combustion
F30	Agricultural land to Import/Export
F31	Horticulture to Air
F32	Horticulture to Water
F33	Horticulture to Waste
F34	Horticulture to Households
F35	Horticulture to Urban green
F36	Horticulture to Import/Export
F37	Urban green to Air
F38	Urban green to Water
F39	Urban green to Waste
F40	Livestock to Air
F41	Livestock to Wastewater
F42	Livestock to Waste
F43	Livestock to Households

F44	Livestock to Agricultural land
F45	Livestock to Industry
F46	Livestock to Import/Export
F47	Pets to Air
F48	Pets to Waste
F49	Pets to Urban green
F50	Pets to Import/Export
F51	Industry to Wastewater
F52	Industry to Waste
F53	Industry to Households
F54	Industry to Agricultural land
F55	Industry to Horticulture
F56	Industry to Urban green
F57	Industry to Livestock
F58	Industry to Pets
F59	Industry to Combustion
F60	Industry to Import/Export
F61	Combustion to Air
F62	Import/Export to Air
F63	Import/Export to Wastewater
F64	Import/Export to Horticulture
F65	Import/Export to Livestock
F66	Import/Export to Pets
F67	Import/Export to Industry
F68	Import/Export to Outside boundaries
F69	Outside boundaries to Import/Export

Appendix B – Inequality constraints of the UNB used to implement the LIM of Vienna surrounding area for the base year 2015.

Flow number	Flow name	Lower bound (kg N.year⁻¹)	Upper bound (kg N.year⁻¹)
F1	Air to Agricultural land	3.15E+06	8.85E+06
F2	Air to Horticulture	1.71E+03	1.93E+03
F3	Air to Urban green	2.12E+05	2.47E+05
F5	Wastewater to Air	1.81E+06	2.97E+06
F6	Wastewater to Water	7.02E+05	9.13E+05
F7	Wastewater to Waste	8.79E+05	8.80E+05
F8	Wastewater to Agricultural land	1.52E+05	1.84E+05
F9	Water to Agricultural land	1.19E+05	1.22E+05
F10	Water to Horticulture	8.26E+02	1.50E+03
F13	Waste to Air	5.41E+05	1.32E+06
F14	Waste to Agricultural land	2.28E+05	5.66E+05
F15	Waste to Urban green	2.78E+05	6.91E+05
F16	Waste to Industry	2.14E+05	3.22E+05
F17	Waste to Combustion	8.50E+05	1.12E+06
F18	Waste to Import/export	7.09E+04	1.03E+05
F19	Households to Wastewater	2.94E+06	3.60E+06
F20	Households to Waste	8.79E+05	1.91E+06
F21	Households to Urban green		1.38E+06
F22	Households to Combustion	1.23E+06	1.31E+06
F23	Agricultural land to Air	1.25E+06	1.66E+06
F24	Agricultural land to Water	3.78E+06	6.76E+06
F25	Agricultural land to Waste	1.75E+05	3.16E+05
F26	Agricultural land to Households		3.82E+06
F27	Agricultural land to Livestock	2.29E+06	4.15E+06
F28	Agricultural land to Industry	4.14E+06	6.38E+06
F29	Agricultural land to Combustion	3.85E+04	4.07E+04
F31	Horticulture to Air	8.75E+02	1.04E+03
F32	Horticulture to Water	2.98E+03	3.72E+03
F34	Horticulture to Households	6.27E+03	8.62E+03
F36	Horticulture to Import/export	4.53E+03	7.25E+03
F37	Urban green to Air	3.30E+05	1.03E+06
F38	Urban green to Water	1.02E+05	3.30E+05
F39	Urban green to Waste		1.12E+06
F40	Livestock to Air	4.04E+05	5.06E+05
F42	Livestock to Waste	1.64E+05	2.98E+05
F43	Livestock to Households	2.93E+05	5.31E+05
F44	Livestock to Agricultural land	1.70E+06	2.15E+06
F45	Livestock to Industry	1.82E+05	3.29E+05
F46	Livestock to Import/export	2.05E+04	3.03E+04
F47	Pets to Air	1.39E+04	1.73E+04

F49	Pets to Urban green	1.94E+05	2.42E+05
F51	Industry to Wastewater	5.67E+05	1.39E+06
F52	Industry to Waste	2.59E+03	5.62E+03
F53	Industry to Households	2.10E+06	6.52E+06
F55	Industry to Horticulture	1.74E+04	2.17E+04
F56	Industry to Urban green	2.69E+04	2.66E+05
F58	Industry to Pets	4.60E+05	5.73E+05
F59	Industry to Combustion		1.52E+07
F60	Industry to Import/export		2.37E+07
F61	Combustion to Air	5.02E+06	8.03E+06
F64	Import/export to Horticulture	8.65E+04	1.32E+05
F65	Import/export to Livestock	6.01E+04	8.72E+04